# Shakedown limit of elbow pipe under coupled cyclic thermal-mechanical loading based on the LMM

Xiaohui Chen[a*], Yang Liu[a,b], Lin Zhu[a], Lang Lang[a], Haofeng Chen[c,d*]

[a]School of Control Engineering, Northeastern University, Qinhuangdao 066004, China

[b]College of Locomotive and Rolling stock Engineering, Dalian Jiaotong University, Dalian, 116028, China

[c]Key Laboratory of Pressure Systems and Safety (DOE), School of Mechanical and Power Engineering, East China University of Science and Technology, Shanghai, 200237, China

[d]Department of Mechanical and Aerospace Engineering, University of Strathclyde, 75 Montrose Street, Glasgow G1 1XJ, Scotland, United Kingdom

*Corresponding author: Xiaohui Chen

Email address: huixiao_chen@126.com

**Abstract**

In this paper, the linear matching method (LMM) is used to study the shakedown limit of elbow pipes under coupled cyclic mechanical-thermal load. Firstly, the thermal stress analyses of elbow pipes under constant internal pressure and cyclic temperature load are carried out. Further, the shakedown limits of the elbow pipes are calculated using the LMM. For the verification purposes, step-by-step inelastic analyses are performed, showing different structure responses under different loading conditions. All the obtained results indicate that the LMM is able to simulate large range of coupled cyclic mechanical-thermal loading conditions with high computational efficiency, and provide shakedown limit with high accuracy. In addition, the effects of bend angles, mean radius to wall thickness ratio ( $r/t$ ) and five load conditions on the shakedown behaviour are also presented.

**Keywords**: Elbow pipe; Linear matching method; Shakedown limit; Mean radius-thickness ratio; Coupled cyclic mechanical-thermal load.

## Nomenclature

### Abbreviations

| | |
|---|---|
| AGR | advanced gas-cooled reactor |
| C-TDF | committee of three dimensional finite element stress evaluation |
| FE | finite element |
| LMM | linear matching method |
| NSM | nonlinear superposition method |
| PEEQ | equivalent plastic strain |
| PEMAG | plastic strain magnitude |
| PWD | plastic work dissipation |
| SCM | stress compensation method |
| TBCs | thermal barrier coatings |
| 2D | two-dimensional |
| 3D | three-dimensional |

### Variables

| | |
|---|---|
| $E$ | Elastic modulus, MPa |
| $L_1$ | length of straight pipe in XY plane, mm |
| $L_2$ | length of straight pipe in XZ plane, mm |
| $L_3$ | length of straight pipe in XY plane, mm |
| $P$ | steady internal pressure, MPa |
| $P_L^s$ | limit internal pressure of the equivalent straight pipe, MPa |
| $r$ | mean radius, mm |
| $r_i$ | inner wall radius, mm |
| $r_o$ | outer wall radius, mm |
| $R$ | bending radius, mm |
| $R_1$ | bending radius of elbow pipe in XY plane, mm |
| $R_2$ | bending radius of elbow pipe in XZ plane, mm |
| $S$ | surface of a volume where loads and boundary conditions are applied |
| $S_u$ | part of the surface where boundary conditions are applied |
| $S_T$ | part of the surface where loads are applied |
| $t$ | wall thickness, mm |
| $t_L$ | current time in the cycle, hours |
| $t_1$ | time for maximum temperature in a cycle, hours |
| $t_2$ | time for minimum temperature in a cycle, hours |
| $\Delta t$ | total cycle time, hours |
| $\Delta u_i^c$ | displacement increment in direction i, mm |
| $\Delta u_j^c$ | displacement increment in direction j, mm |
| $\dot{u}_i$ | displacement rate, mm/s |
| $V$ | volume of an ideal elasto-plastic structure |
| $x$ | location within the volume, V |
| $\alpha$ | bending angle of elbow pipe in XY plane, ° |
| $\beta$ | bending angle of elbow pipe in XZ plane, ° |
| $\delta_{ij}$ | displacement component, mm |
| $\Delta\varepsilon_{ij}^c$ | compatible strain increment |

| | |
|---|---|
| $\dot{\varepsilon}_{ij}$ | plastic strain rate |
| $\dot{\varepsilon}_{ij}^{c}$ | admissible strain rate history |
| $\bar{\dot{\varepsilon}}$ | effective strain rate |
| $\lambda$ | load multiplier |
| $\lambda_{LB}$ | lower bound shakedown load parameter |
| $\lambda_{P}$ | thermal load multiplier |
| $\lambda_{S}$ | precise upper bound shakedown multiplier |
| $\lambda_{UB}$ | upper bound shakedown load parameter |
| $\lambda_{LB}^{s}$ | precise lower bound shakedown multiplier |
| $\lambda_{\theta}$ | thermal load multiplier |
| $\dot{\mu}$ | plastic multiplier |
| $v$ | Poisson's ratio |
| $\theta_{0}$ | outer wall temperature, ℃ |
| $\Delta\theta$ | temperature load change amount, ℃ |
| $\Delta\theta_{0}$ | temperature gradient, ℃ |
| $\sigma_{ij}$ | stress component, MPa |
| $\sigma_{ij}^{c}$ | stress at yield associated with admissible strain rate history, MPa |
| $\sigma_{ij}'$ | deviatoric stress at yield, MPa |
| $\sigma_{y}$ | yield stress, MPa |
| $P$ | mechanical load |
| $\theta$ | thermal load |
| $\rho_{ij}^{r}$ | varying residual stress, MPa |
| $\bar{\rho}_{ij}$ | constant residual stress, MPa |
| $\bar{\sigma}$ | effective (Von-Mises) value of the stress in the bracket, MPa |
| $\hat{\sigma}_{ij}$ | linear elastic solution history |
| $\hat{\sigma}_{ij}^{P}$ | elastic solution of mechanical load |
| $\hat{\sigma}_{ij}^{\theta}$ | elastic solution of thermal load |

## 1. Introduction

Pipeline networks, mainly consist of elbow and straight pipe structures, play an important role in numerous fields, for example the pharmaceutical industry, nuclear and conventional power plants. To design piping networks efficiently, elbow pipes become essential components for changing the direction of the fluid and provide necessary flexibility for the entire pipeline by accommodating the changes of temperature and/or mechanical loads. However, structural integrity assessment of elbow pipes is so sophisticated because of the curved geometry [1-3]. Shakedown analysis is widely used in reliability design and assessment of components subjected to alternating loads. Xu et al. [4] took the thick-walled cylinder as research object and adopted the unified strength criterion to perform shakedown analysis under internal pressure. Oh et al. [5] used finite element (FE) analysis for investigating limit loads of pressured 90° elbow pipes under cyclic bending moment which shows good agreement with the Bree diagram. Similarly, taking the 90° back-to-back elbow pipes as research object, Abdalla et al. [6] adopted direct non–cyclic simplified technique to investigate the elastic shakedown limits of elbow pipe under a series of certain load conditions and the results coincide with the FE simulations. On this basis, comparing to the elbow pipes under in-plane bending moments, Oda [7] further investigated shakedown limits of 90° pressurized elbows under relative bending moments, the results show higher shakedown zones and better accommodation of loads. In addition, Abdalla et al. [8] successfully verified the accuracy of the elastic shakedown limit pressures estimated by the Nonlinear Superposition Method (NSM) using the experimental method of cementing strain gauges to the spherical vessels with nozzles. Do et al. [9] presented a more reliable and efficient isogeometric FE method for estimating ultimate loads and shakedown limit loads of pressure vessels, and applied this method to example analysis, such as nozzle and skirt of pressure vessel. Currently, Abdalla [10] presented a methodology to determine the shakedown limit loads by calculating the plastic work dissipation (PWD). The advantage of this method is that it can combine the large displacement equation and/or the cyclic plasticity constitutive material model, and is accessible to accurately distinguish between the shakedown and non-shakedown responses.

With using the above methods, the load conditions in shakedown analysis of the structure or components are limited to be mechanical loads such as pressures and bending moments, and the temperature loads cannot be considered. However, temperature, especially high-temperature load condition, is a factor affecting the integrity of structures or components in many practical engineering fields, and cannot be ignored. Considering the extension of the static shakedown theorem to the plastic field, Adibi-Asl et al. [11, 12] proposed ratchet boundary calculation equation with non-cyclic method, and determined ratchet boundary of thin plate and holed plate under different coupled mechanical-thermal loads. Simon et al. [13] utilized the Melan's static shakedown theorem for determining elastic and shakedown limits of nozzle in a certain pressure vessel. And the results of multiple independent variable load interactions including temperature were obtained and compared with results from other research works. At present, the more mature method for high-temperature structural integrity assessment is LMM. Chen et al. [14 -16] has studied structures and components such as plate under biaxial loading with a hole, pipeline under coupled mechanical loads with defect, 2D tubeplate at the outlet from a typical AGR heat exchanger and complex 3D tubeplate in a typical AGR superheater header, and confirmed the applicability of LMM to complex 3-D structures. A series of numerical analytical methods based on the LMM is presented, and successively developed the LMM as an efficient method for evaluating the response of structures under high temperature loads. After that, Chen et al. [17] used LMM for investigating shakedown limits of a 3D hole-plate under combined mechanical-thermal load, and the results were compared with those of procedures already existed, demonstrating good applicability of LMM to typical cases. Zhu et al. [18] used LMM to perform shakedown and ratchet analysis of steam turbine rotor under coupled cyclic mechanical-thermal loads, and gave Bree-like diagrams to calculate plastic strain range. Gong et al. [19] took the pipeline with an oblique nozzle which operates in power plant as research object, also investigated the shakedown limits of it subjected to pressure and alternative temperature inside the structure with LMM. The outcomes indicate that the LMM is capable to distinguish different structure responses. As the load conditions under consideration become more and more complex, the traditional Bree diagram has certain limitations, and some scholars have already turned their attention to the new form of Bree diagram. Cho et al. [20] added a coordinate axis to the 2D Bree diagram, thereby introducing a new load condition, and used the LMM for giving the shakedown limit of a specific 90° elbow pipeline under three cyclic mechanical-thermal load paths. The new form of shakedown limit is more comprehensive than the traditional Bree diagram. In addition to its important role in structural assessment, the LMM also extends into other related fields. Noting that TBCs (Thermal barrier coatings) operating in high-temperature environments initiate cracks at microscopic defects owing to the complex structures, Zheng et al. [21] utilized the LMM to give the shakedown limits of TBCs with interface defects and proposed a shakedown numerical analytical method for TBCs. Ma et al. [22] complemented and extended the LMM by taking into account limited kinematic hardening and non-isothermal effect, and applied the new method to the shakedown analysis of a turbine disk to demonstrate the good generality of the method. Besides the LMM, the SCM developed by Peng et al. [23] can bypass the complicated calculations and greatly improve the efficiency. The method had been already used for the shakedown assessment of a certain typical pressure vessel structure, also taking into account the independently varying load circumstances and non-isothermal effect, and had been demonstrated to give 2D and 3D shakedown limits of the component.

At the same time, the presence or absence of structural or component defects, the influence of dimensional parameter and shape changes on the shakedown limit are also important research contents in the shakedown analysis. Studying these factors will help determine the reasonable shape and size of the structure or component under a certain load condition. Oh et al. [5] systematically investigated the influence of the ratio of typical geometric dimensions and geometric variation of elbow pipe on the shakedown limits. While due to the complexity of the limit loads, only general regularities were given. Oda et al. [7] investigated the impacts of thinning location and depth on the shakedown limits of 90° elbow pipe, and gave the thinning location that severely decreased the shakedown domain. Gong et al. [19] pointed out that the ratchet and reverse plasticity limits show totally different trends for the angle variation of oblique nozzle, and that the thickness of each component has a great influence on the shakedown limit. Cho et al. [20] investigated the shakedown limits of 90° elbow pipes with different geometrical characteristics under two cyclic loading conditions, and gave the load adaptability and applicability of each geometrical characteristic. Zheng et al. [21] observed that the depth of defects is a key factor influencing the shakedown limit of TBCs, the deeper the defects, the smaller the shakedown limit loads. Balakrishnan et al. [24] included the ovality formed due to the bend of the 90° elbow pipe itself into research scope, and also considered the thinning factor, both of which have gradient changes. The research work gave the shakedown limits of the elbow under coupled mechanical load by utilizing direct non-cyclic simplified technique. And the results indicate that the ovality is a key factor influencing the shakedown domain under same conditions. Chen et al. [25] presented the effects of typical geometry characteristics $R/r$ and $r/t$ of 90° pressured elbow pipes subjected to cyclic bending moments on shakedown limits by using LMM. Chen et al. [26] investigated the ratcheting effect and ratcheting limit of a certain pressured thinning structure subjected to bending moments with C- TDF (The Committee of Three Dimensional Finite Element Stress Evaluation) and LMM. It has been observed that the depth, length and circumferential angles of defect have obvious influences on the ratcheting behavior of structure.

In this study, the LMM is used to determine the shakedown limit of the 90° and 135° elbow pipe. In order to verify the accuracy of the LMM, the obtained outcomes are validated by using Abaqus step-by-step method. The influences of various effects such as bending angles, mean radius - thickness ratio and loading paths on the shakedown limit of the elbow pipe are studied using the LMM.

## 2. Basic numerical procedure for the LMM

Chen et al. [25] discussed in detail the numerical analytical method of LMM shakedown analysis. Supposing that the convexity of yield condition is under consideration, the elastic modulus $E$ and Poisson's ratio $v$ do not consider the non-isothermal effect, and the relevant flow rule applies

$$\dot{\varepsilon}_{ij} = \dot{\mu}\frac{\partial f}{\partial \sigma'_{ij}} \tag{1}$$

where $\dot{\varepsilon}_{ij}$ is strain rate, $\sigma'_{ij} = \sigma_{ij} - \frac{1}{3}\sigma_{ij}\delta_{ij}$ is the deviatoric stress and $\dot{\mu}$ is a plastic multiplier. The von Mises condition assumed by the shakedown theorems is shown as

$$f\left(\sigma_{ij}\right) = \bar{\sigma}\left(\sigma_{ij}\right) - \sigma_y = 0 \tag{2}$$

where $\sigma_y$ is yield stress of the material, $\bar{\sigma}\left(\sigma_{ij}\right)$ is the von Mises effective stress, which is calculated by

$$\bar{\sigma}\left(\sigma_{ij}\right) = \sqrt{\frac{3}{2}\sigma'_{ij}\sigma'_{ij}} \tag{3}$$

Assuming that there is an ideal elasto-plastic structure which satisfies von-Mises yield criterion. Its volume is V and surface area is S. A coupled cyclic mechanical-thermal load is applied to the structure in cycle time $0 \le t \le \Delta t$, where thermal load, $\lambda_\theta \theta\left(x,t\right)$, is distributed over the entire volume. The mechanical load, $\lambda_P P\left(x,t\right)$, acts on a portion of the surface, $S_T$. The rest of the surface, $S_u$, is considered to have a rate of displacement $\dot{u}_i = 0$. $\lambda$ is a loading multiplier that can vary the magnitude of the load in order to consider a larger range of cyclic loads. Corresponding to the coupled cyclic loads, the linear-elastic stress solution $\lambda\hat{\sigma}_{ij}$ is shown as

$$\lambda\hat{\sigma}_{ij}\left(x,t\right) = \lambda_\theta\hat{\sigma}^{\theta}_{ij}\left(x,t\right) + \lambda_P\hat{\sigma}^{P}_{ij}\left(x,t\right) \tag{4}$$

where $\lambda_\theta$ is a thermal load multiplier, $\lambda_P$ is a mechanical load multiplier. $\hat{\sigma}^{\theta}_{ij}\left(x,t\right)$ is the elastic solution of $\theta\left(x,t\right)$ and similarly $\hat{\sigma}^{P}_{ij}\left(x,t\right)$ is the elastic solution of $P\left(x,t\right)$. For any cyclic problem, continuous application of these loads will result in the following stress fields in the component

$$\sigma_{ij}\left(x,t\right) = \lambda\hat{\sigma}_{ij}\left(x,t\right) + \bar{\rho}_{ij}\left(x\right) + \rho^{r}_{ij}\left(x,t\right) \tag{5}$$

where $\bar{\rho}_{ij}\left(x\right)$ and $\rho^{r}_{ij}\left(x,t\right)$ are a constant residual stress field and a varying residual stress, respectively. If any changes occur in the load history, $\rho^{r}_{ij}\left(x,t\right)$ describes the changes and satisfies

$$\rho_{ij}^{r}\left(x,0\right)=\rho_{ij}^{r}\left(x,\Delta t\right) \tag{6}$$

For shakedown analysis, $\rho_{ij}^{r}\left(x,t\right)=0$ needed be satisfied owing to the nature of self-equilibrating from residual stresses. Therefore, the cyclic stress history is completely described by the applied cyclic stresses and residual stress field independent of time

$$\sigma_{ij}\left(x,t\right)=\lambda\hat{\sigma}_{ij}\left(x,t\right)+\bar{\rho}_{ij}\left(x\right) \tag{7}$$

In order to establish the connection between incompressible and kinematically admissible strain rate history $\dot{\varepsilon}_{ij}^{c}$ and displacement, a compatible strain increment $\Delta\varepsilon_{ij}^{c}$ needs to be introduced, such that

$$\int_{0}^{\Delta t}\dot{\varepsilon}_{ij}^{c}dt=\Delta\varepsilon_{ij}^{c} \tag{8}$$

The displacement increment field is introduced and associated with $\Delta\varepsilon_{ij}^{c}$. This displacement increment field conforms to the displacement boundary condition, so the strain-displacement relations is shown as

$$\Delta\varepsilon_{ij}^{c}=\frac{1}{2}\left(\frac{\partial\Delta u_{i}^{c}}{\partial x_{j}}+\frac{\partial\Delta u_{j}^{c}}{\partial x_{i}}\right) \tag{9}$$

Considering the coupled cyclic mechanical-thermal load, the upper bound shakedown theorem is shown below

$$\lambda_{UB}\int_{V}\int_{0}^{\Delta t}\left(\hat{\sigma}_{ij}\dot{\varepsilon}_{ij}^{c}\right)dtdV=\int_{V}\int_{0}^{\Delta t}\sigma_{ij}^{c}\dot{\varepsilon}_{ij}^{c}dtdV \tag{10}$$

where $\lambda_{UB}$ represents the upper bound shakedown load parameter which can scale the load, so it is also a linear solution. $\sigma_{ij}^{c}$ and $\hat{\sigma}_{ij}$ are the yield stress and linear solution associated with $\dot{\varepsilon}_{ij}^{c}$ and coupled cyclic load history, respectively.

For simplification purposes, Eq. (1) is rewritten in terms of the Prandtl-Reuss relation as

$$\dot{\varepsilon}_{ij}=\frac{3}{2}\left(\frac{\dot{\bar{\varepsilon}}}{\sigma_{y}}\right)\sigma_{ij}',\dot{\varepsilon}_{kk}=0 \tag{11}$$

where $\dot{\bar{\varepsilon}}=\sqrt{\frac{2}{3}\dot{\varepsilon}_{ij}\dot{\varepsilon}_{ij}}$ is the effective strain rate.

Therefore, Eq. (10) can be simplified by combining the relevant flow rule,

$$\lambda_{UB} = \frac{\int_V \int_0^{\Delta t} \sigma_y \bar{\dot{\varepsilon}}\left(\dot{\varepsilon}_{ij}^c\right) dt dV}{\int_V \int_0^{\Delta t} \left(\hat{\sigma}_{ij} \dot{\varepsilon}_{ij}^c\right) dt dV} \tag{12}$$

when the following inequality hold constant

$$\lambda_{UB} \geq \lambda_S \tag{13}$$

After consecutive iterations, $\lambda_S$ is the precise shakedown multiplier obtained by converge to the least upper bound.

Chen et al. [27] introduced the static shakedown theorem into the LMM to calculate the lower bound shakedown limit and gave the following equation

$$\begin{aligned} &\lambda_{LB}^s = \max \lambda_{LB} \\ s.t. \quad & f\left(\lambda_{LB} \hat{\sigma}_{ij}(x,t) + \bar{\rho}_{ij}(x)\right) \leq 0 \end{aligned} \tag{14}$$

**3. Finite element model**

*3.1 Geometric model of the pipeline*

In this study, the pipeline is taken as the object of investigation, and its geometry is shown in Fig. 1, where $r_i$, $r_o$, and $r$ represent the inner wall radius, outer wall radius and mean radius of the pipeline, respectively. For each straight pipe in two elbow pipes, the corresponding length is $L_1$ = 1800 mm, $L_2$ = 400 mm, $L_3$ = 1400 mm, respectively. The bending radius of the elbow pipes represents $R_1$ = 700 mm and $R_2$ = 600 mm, respectively. The parameters $\alpha$ and $\beta$ represent the bending angle of two elbow pipes, respectively. And Table 1 lists the geometrical dimensions of the pipeline.

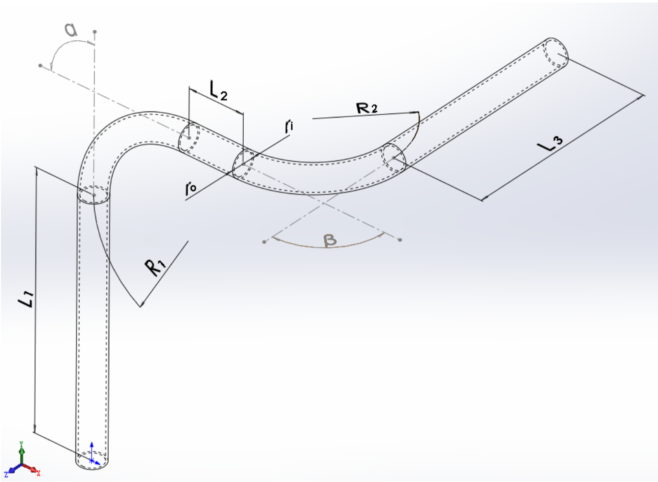


Fig. 1 Geometrical dimensions of the pipeline

Table 1 Geometrical dimensions of the pipeline

| No. Pipeline | $L_1$ /mm | $L_2$/mm | $L_3$/mm | $R_1$/mm | $R_2$/mm | $r_i$/mm | $r_o$/mm | $r$/mm | $\alpha$ | $\beta$ |
|---|---|---|---|---|---|---|---|---|---|---|
| ① | 1800 | 400 | 1400 | 700 | 600 | 77 | 91 | 84 | 90° | 90° |
| ② | 1800 | 400 | 1400 | 700 | 600 | 133 | 147 | 140 | 90° | 90° |
| ③ | 1800 | 400 | 1400 | 700 | 600 | 203 | 217 | 210 | 90° | 90° |
| ④ | 1800 | 400 | 1400 | 700 | 600 | 77 | 91 | 84 | 135° | 135° |

*3.2 Finite element model*

Fig. 2 shows the finite element model constructed by ABAQUS according to the geometric dimensions of elbow pipe (Fig.1). The 20-node quadratic heat transfer brick (DC3D20) element is first adopted as the temperature factor is involved. There are 17, 520 20-node quadratic bricks with reduced integration technique (C3D20R) adopted for the stress field analysis. Fig. 2 also indicates the finite element meshing of the pipeline. After conducting a study on meshing with a view to obtain results efficiently and accurately, the pipeline is configured with 15,760 elements for meshing and there are two layers of meshes in the thickness direction. Table 2 lists the material parameters of the pipeline.

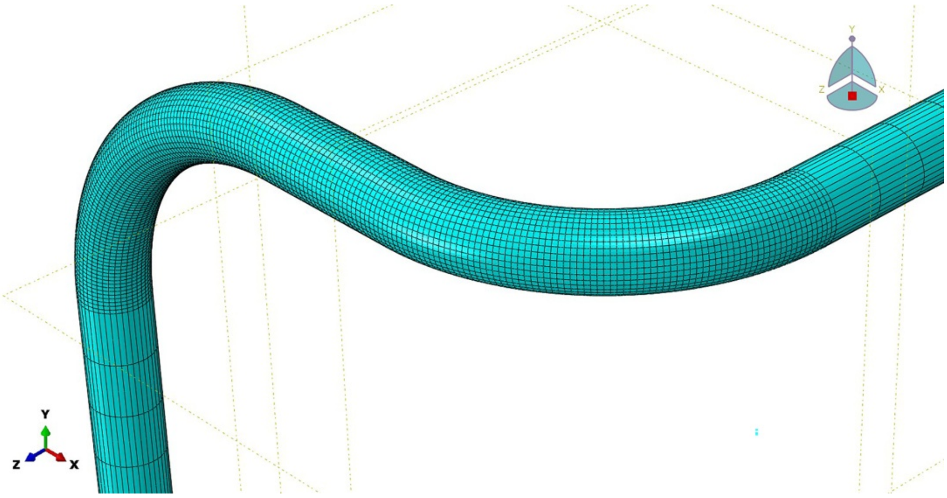


Fig. 2 Finite element model

**Table 2** Material parameters

| Elastic modulus $E$/MPa | Poisson's ratio ν | Yield stress $\sigma_y$/MPa | Thermal expansion coefficient | Thermal conductivity /(W/(m*K)) |
|---|---|---|---|---|
| 201660 | 0.3 | 360 | 1e-005 | 20 |

*3.3 Loading and boundary conditions*

The coupled cyclic mechanical-thermal load history applied to the pipeline model is shown in Fig. 3. The temperature reaches the maximum value of the cycle history at $t_1$ and decreases to the minimum temperature at $t_2$, as shown in Fig.3(a). Fig.3(b) shows constant internal pressure.

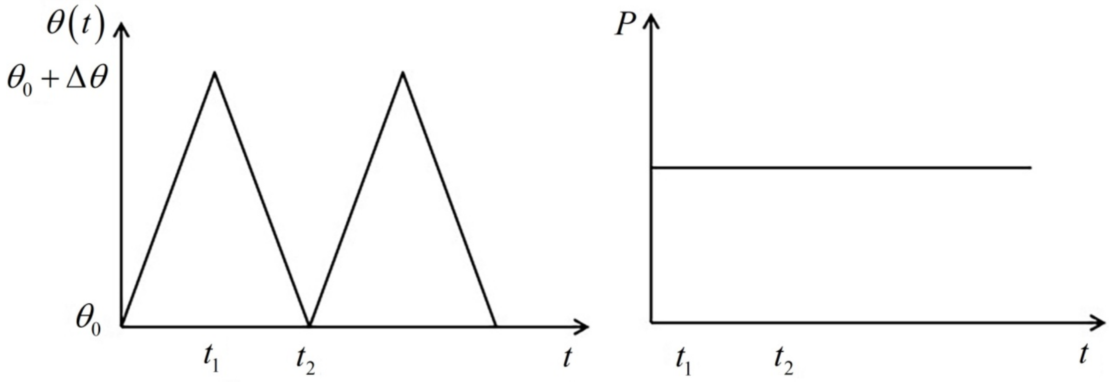


(a) (b)

Fig. 3 Load condition 1

The bottom face is constrained using kinematic coupling. In all movements, only the expansion/contraction of the nodes in the axial direction is prohibited. The straight pipe's free end is applied plane end condition in order to give it the ability to simulate in-plane expansion over the length of the thermal expansion. The coupled cyclic mechanical-thermal load is considered including a 100 MPa internal pressure. Meanwhile, considering the influence of the closed-end condition on the simulation results, the axial stress at the free end of the straight pipe section should be simulated by the equivalent axial tension.

*3.4 Thermal stress analysis*

In this study, Fig. 4 gives the temperature distribution contour, namely the outer wall temperature $\theta_0$=0°C, $\Delta\theta$=$\Delta\theta_0$=800°C, where $\Delta\theta$ is the temperature load change amount and $\Delta\theta_0$ is the temperature gradient. Obviously, the temperature field in Fig. 4 uniformly distribute along the wall thickness direction after the predefined temperature field is added to the model and the maximum temperature of 800°C covers the entire pipeline's inner wall.

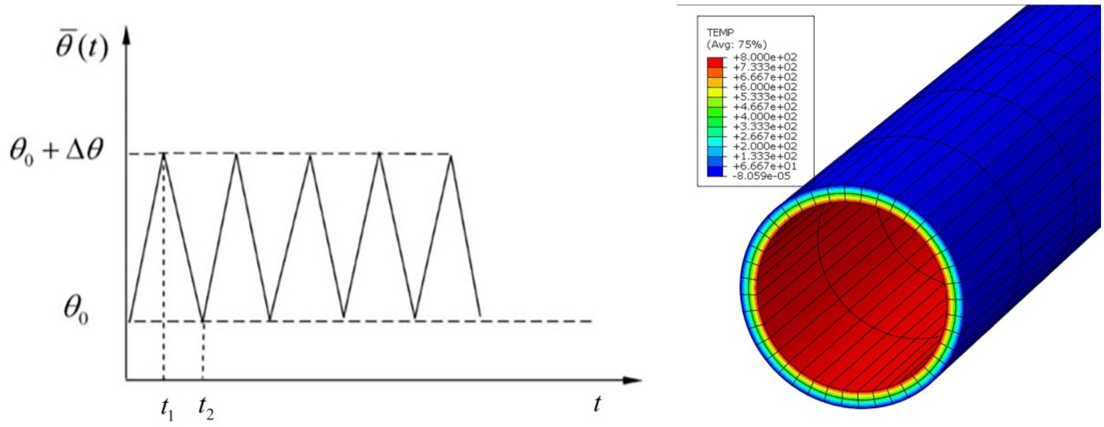


(a) (b)

Fig. 4 Temperature load history and temperature distribution

The thermal stress of the 90° elbow pipes is given in Fig. 5. The stress is mainly concentrated on the intrados of elbow. Fig. 6 gives the displaced and undisplaced contour of the elbow pipes.

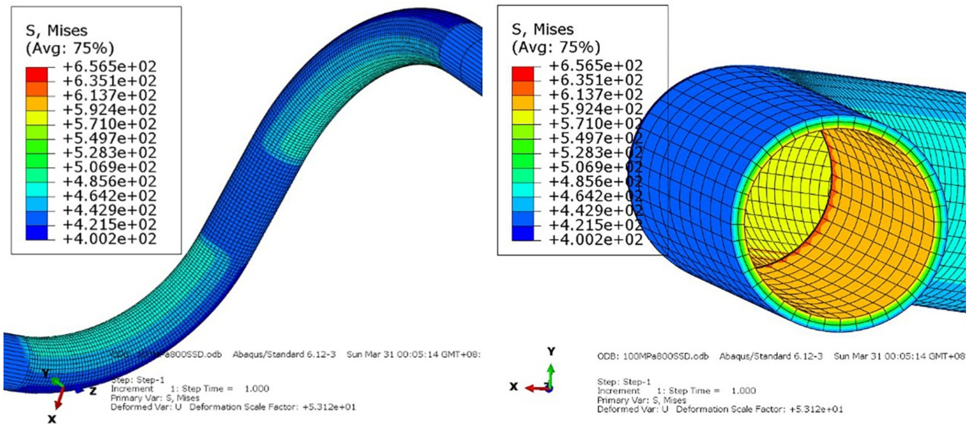


(a) (b)

Fig. 5 Thermal stress contour of the elbow pipes

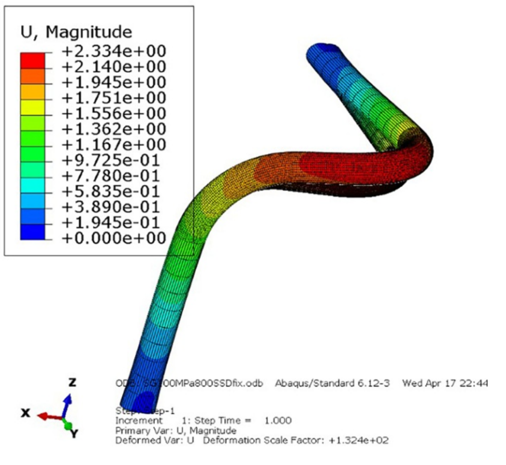


Fig. 6 Displaced and undisplaced contour of the elbow pipes

## 4. Shakedown analysis of elbow pipes

### *4.1 Shakedown limit*

The kinematic theorem and static shakedown theorem are the theoretical basis for the LMM calculation of the upper and lower shakedown bound limits, respectively. These two theorems guide the numerical analytical method to accurately determine each limit multiplier [27]. Considering various loading combinations of cyclic temperature $\Delta\theta$ and steady internal pressure *P*, the shakedown limit of the elbow pipe was calculated using the LMM method. Fig. 7 shows all converged values of shakedown limit multipliers and is also an interaction diagram of shakedown limit for the elbow pipes under load condition 1. The applied mechanical load in X-axis is normalized by the limit internal pressure of the equivalent straight pipe, $P_L^s$. While the loading in Y-axis is normalized by temperature gradient $\Delta\theta_0$=800 °C. The specific calculation method of $P_L^s$ in the reference [25] is shown as:

$$P_L^s = \frac{2}{\sqrt{3}}\sigma_y \ln\left(\frac{r_o}{r_i}\right) \tag{15}$$

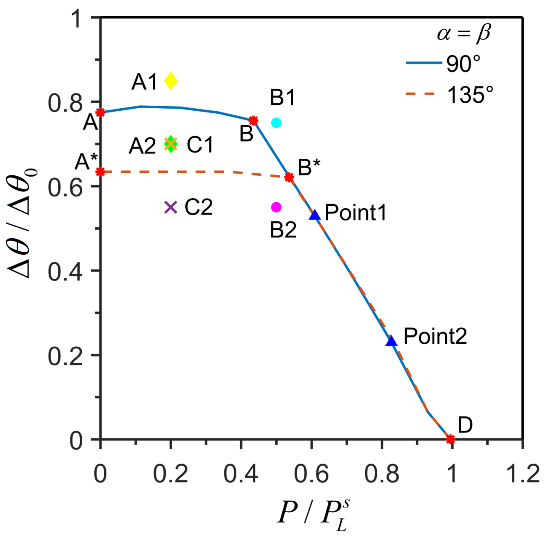


Fig. 7 Shakedown limits of 90° and 135° elbow pipes under Load condition 1

According to the Bree diagram, Fig. 7 consists of two specific domains: the shakedown zone dominated by elastic behavior and the non-shakedown zone dominated by plastic behavior. Further, the non-shakedown domain can be divided into alternating plasticity domain with the strain entering a closed loop and ratchetting domain with the infinite increase of the plastic strain based on the strain-stress hysteresis curve. AB/A*B* is the reverse plasticity limit which signify the transition from elastic shakedown behaviour to reverse plasticity, and BD/B*D is the ratchet limit which signify the transition from elastic shakedown behaviour to ratchetting. There will be no elastic shakedown when the coupled cyclic mechanical-thermal load applied exceeds these two limits which intersect at point B or point B*. The point D corresponds to the limit load of internal pressure imposed without cyclic temperature load. Obviously, there is a significant difference between the reverse plasticity limits of the 90° and 135° elbow pipes. Therefore, the two pipelines will exhibit completely different behavior for loads that are between AB and A*B*.

*4.2 Shakedown analysis of practical operation load cycle*

Load Point 1 and load Point 2 are the results of typical lower and upper bound sequence converging after 20 iterations (Fig. 7). It can be observed from Fig.7 that the convergence of shakedown limits proves the accuracy of the results obtained by LMM. Point1 (0.6095, 0.5290) and Point2 (0.8273, 0.2298) are two load instance points of the shakedown limit of the 90° elbow pipes, and the convergence process of upper and lower shakedown limit multipliers in iterative analysis of the two points are shown in Fig. 8.

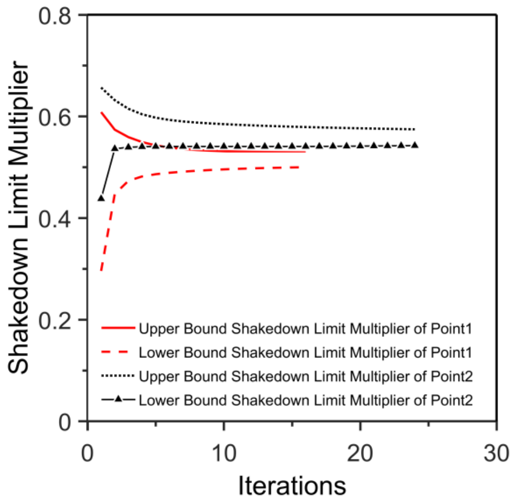


Fig. 8 The process of convergence for upper and lower shakedown iterative analysis

Fig. 9 and Fig. 10 show the steady state effective stress and strain contours of the 90° elbow pipes at Point 1 and Point 2, respectively. Obviously, the coupled cyclic mechanical-thermal load produces the maximum steady state effective strain on the side of intrados of elbow's outer surface and the maximum steady state effective stress on the side of intrados of elbow's inner wall. The difference between the steady state effective strain on the side of intrados of elbow's outer wall at Point 1 and Point 2 is obvious.

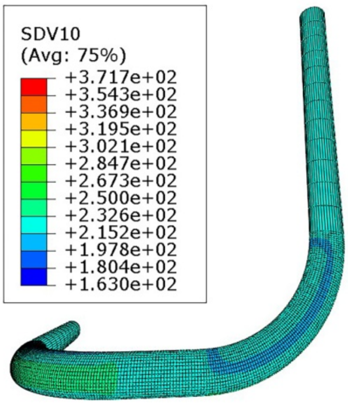


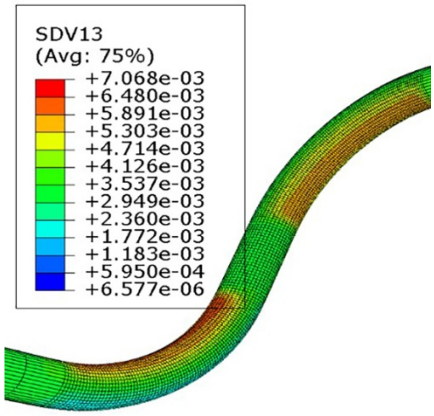


(a) Steady state effective stress in outer wall (b) Steady state effective strain in outer wall

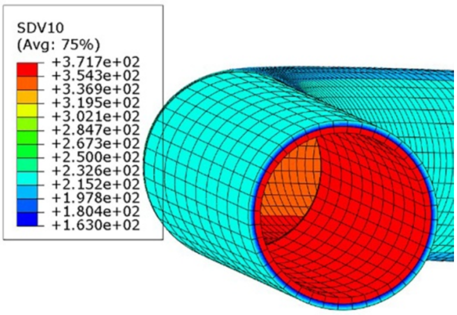


(c) Steady state effective stress in inner wall

Fig. 9 Steady state effective stress and strain contour of Point 1

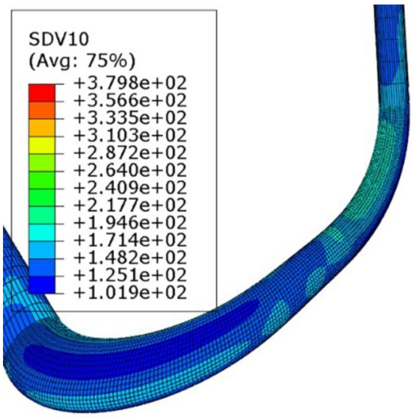


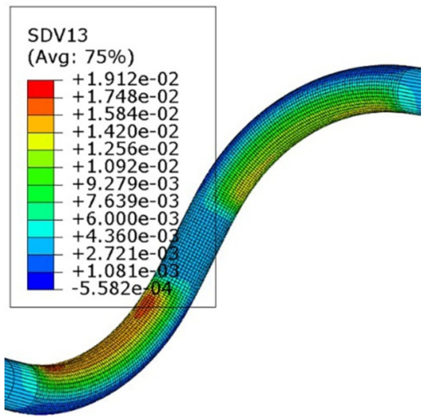


(a) Steady state effective stress in outer wall (b) Steady state effective strain in outer wall

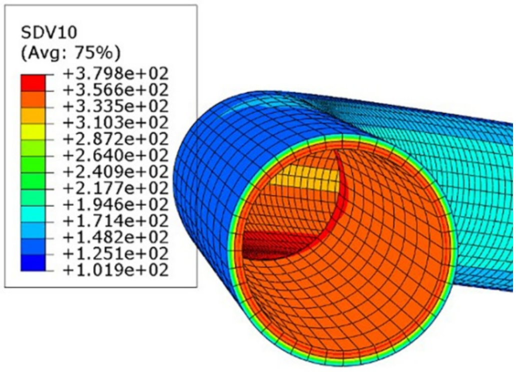


(c) Steady state effective stress in inner wall

Fig. 10 Steady state effective stress and strain cloud diagrams of Point 2

*4.3 ABAQUS step-by-step inelastic analysis*

In order to verify the correctness of the LMM, ABAQUS step-by-step inelastic analysis is performed for analyzing six load instance points (A1- C2) in Fig. 7. In Reference [25], Chen et al. proved the accuracy and reliability of results computed by the LMM by showing an error rate of less than 1% from the Abaqus Riks analysis. The relationship between the magnitude of the plastic strain and the number of cycles at each load instance point is shown in Fig. 11. The use of Plastic Strain Magnitude (PEMAG) to depict the plastic strain incremental history instead of Equivalent Plastic Strain (PEEQ) is because PEMAG gives the correct total plastic strain accumulation by taking into account the signs of plastic strain during the evolution. The largest PEMAG value among the eight Gaussian integration points determines the plastic strain incremental history for different load instance points.

The load instance points A2, B2 and C2 are located on the inner side of the corresponding reverse plasticity limits (AB/A*B*), so the elbow pipe exhibits the elastic shakedown response. Conversely, the elbow pipes under load instance point A1, B1, and C1 exhibits the reverse plasticity response. Both points B1 of the 90° and 135° elbow pipe show the ratchetting response that the plastic strain accumulating up with each loading cycle. Specifically, load instance point B1 is located on the outside of the ratchet limit (BD and B*D), so that both the 90° and 135° elbow pipes exhibit the ratchetting response in which plastic strain accumulates with the number of cycles.

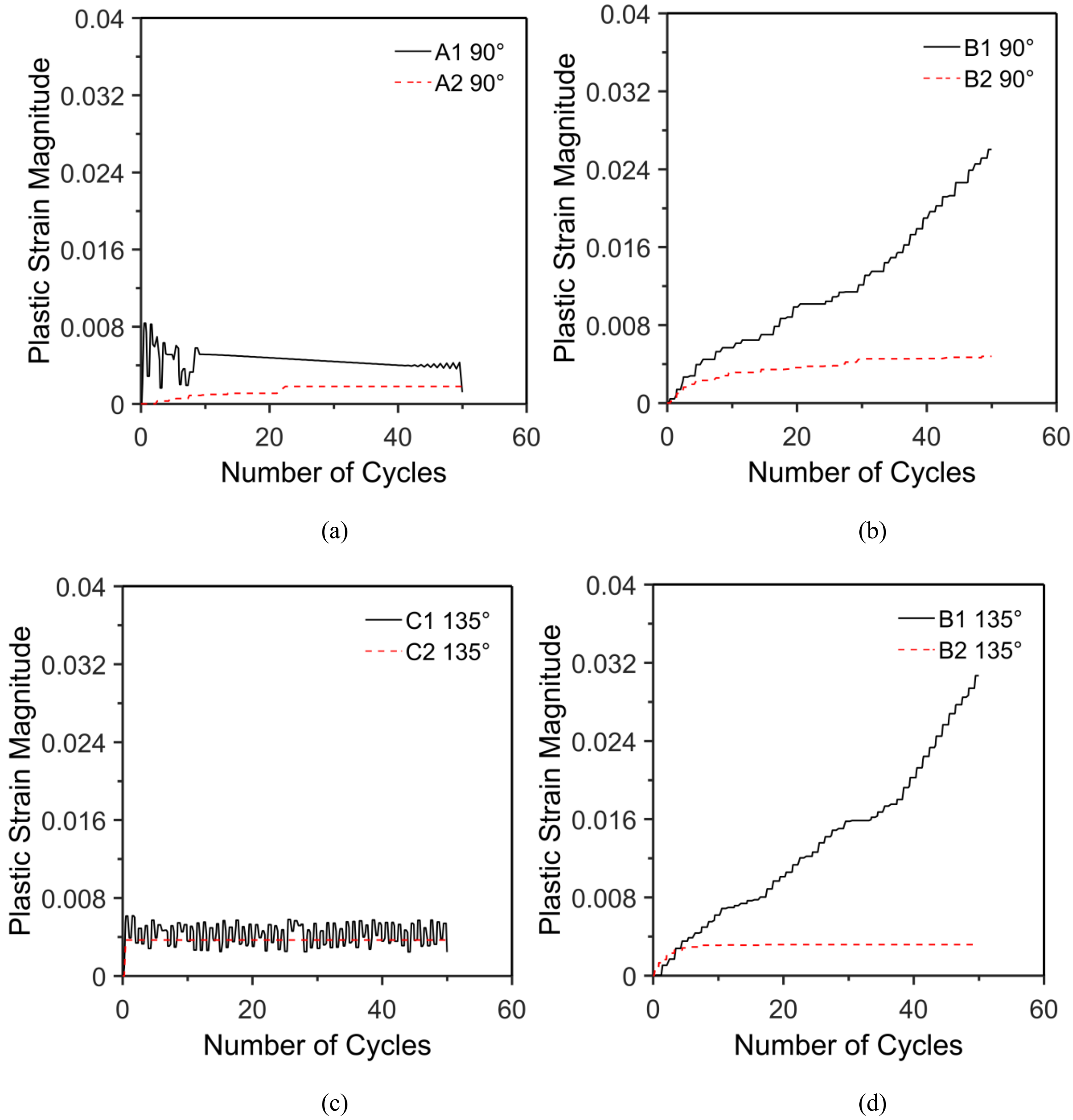


Fig. 11 ABAQUS verification using step by step non-linear analysis

**5. Effects of different factors on shakedown limits**

In this study, the thermal-mechanical loading is classified into five combined load case; Loading condition 1: cyclic thermal loading with triangular waveform and constant internal pressures, Loading condition 2: cyclic thermal load with trapezoidal waveform and constant internal pressures, Loading condition 3: cyclic thermal load with triangular waveform and cyclic internal pressures with triangular waveform, Loading condition 4: cyclic thermal loading with triangular waveform and cyclic internal pressures with trapezoidal waveform and Loading condition 5: cyclic thermal loading with trapezoidal waveform and cyclic internal pressures with triangular waveform. These five coupled cyclic load conditions and the specific loading history of them are shown in the follows.

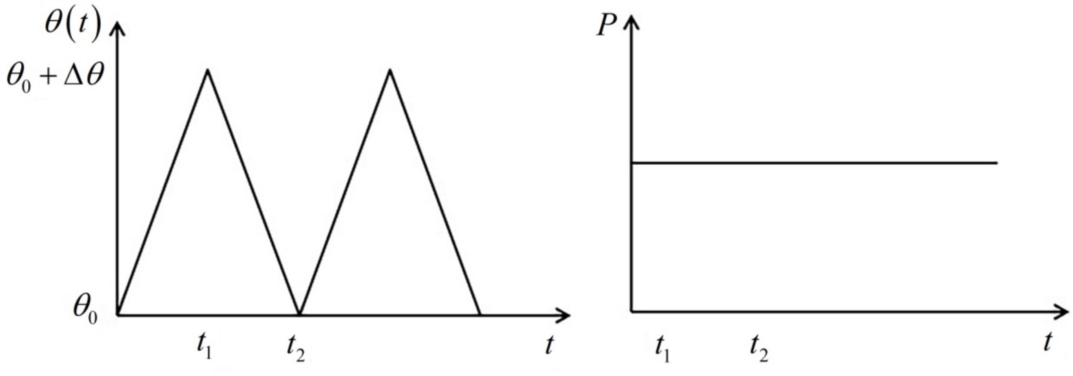


(a) (b)

Fig. 12 Load condition 1

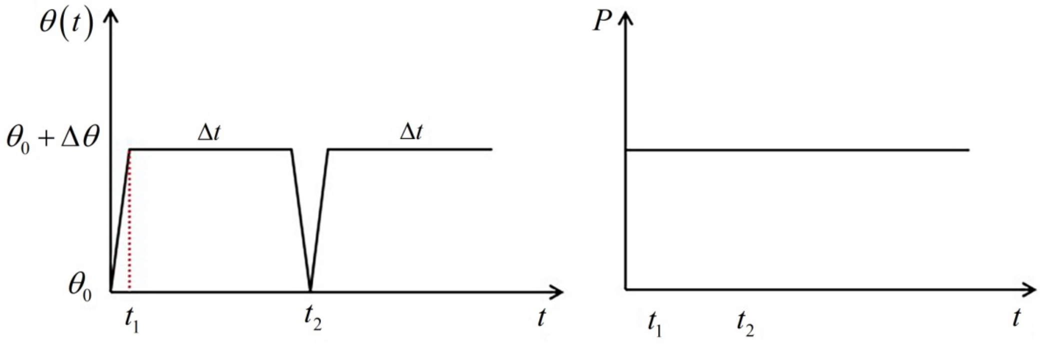


(a) (b)

Fig. 13 Load condition 2

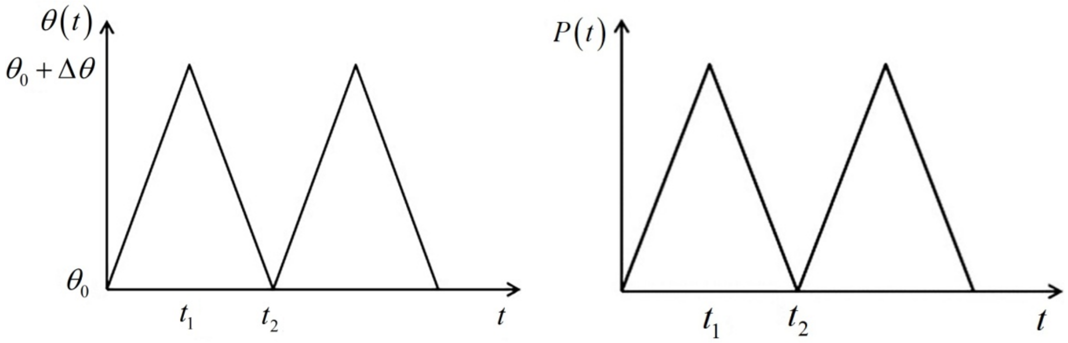


(a) (b)

Fig. 14 Load condition 3

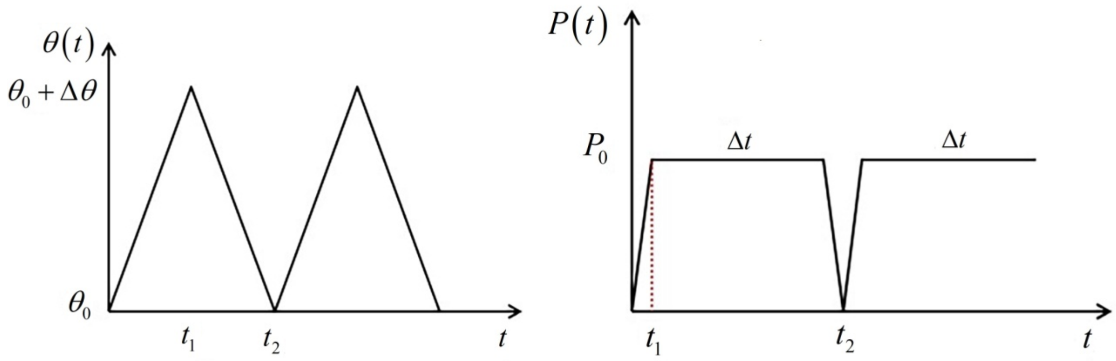


(a) (b)

Fig. 15 Load condition 4

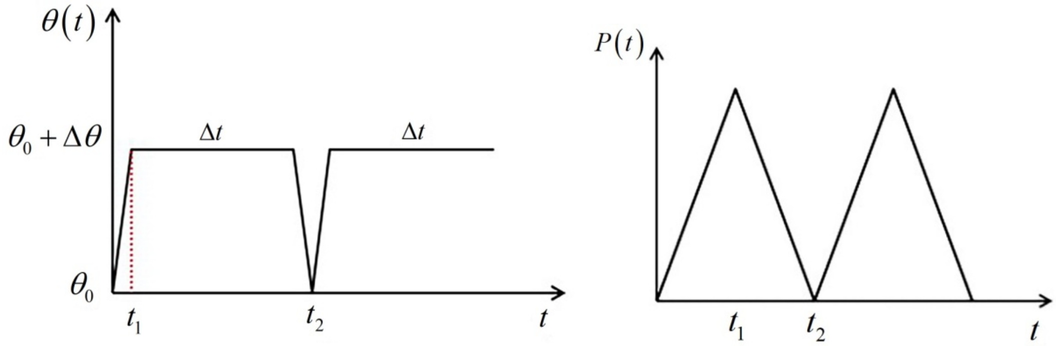


(a) (b)

Fig. 16 Load condition 5

*5.1 Effect of bending angles on shakedown limits*

Fig. 17 shows the shakedown limits of the 90° and 135° elbow pipes under the load condition 2 - load condition 5, respectively. Under the same loading conditions, the general trend for each geometry considered is similar. A clear trend is seen in which the normalised temperature increases with bending angles. The shakedown limits of the 90°elbow pipes under the load conditions 2, 4 and 5 are smaller than those of the 135° elbow pipes. However, the shakedown limits of the 135° elbow pipes under the load condition 3 are smaller than those of the 90° elbow pipes. This is attributed to the temperature and internal pressure without dwell loading.

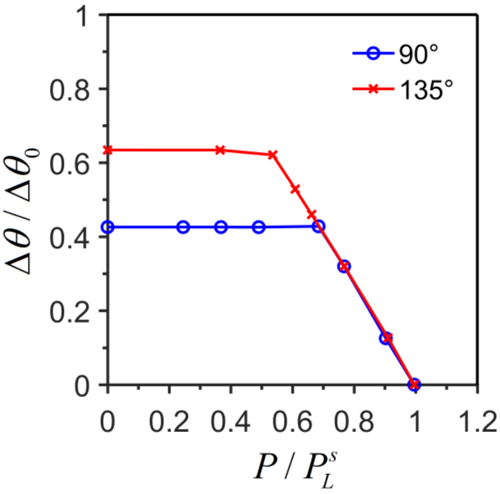


(a) Load condition2

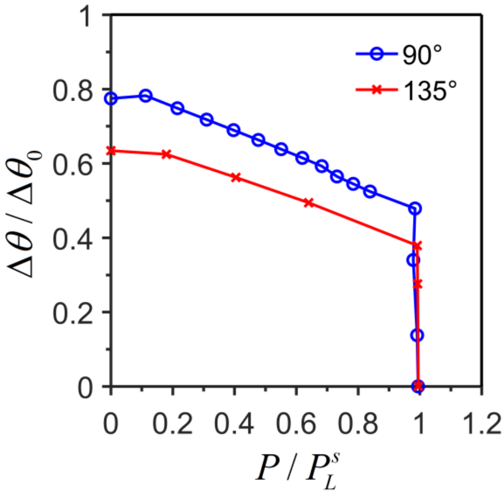


(b) Load condition 3

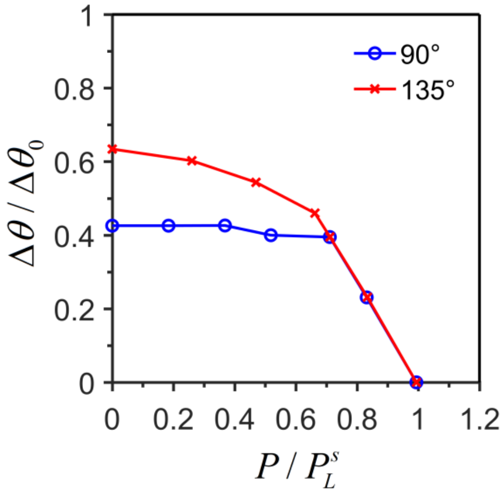


(c) Load condition 4

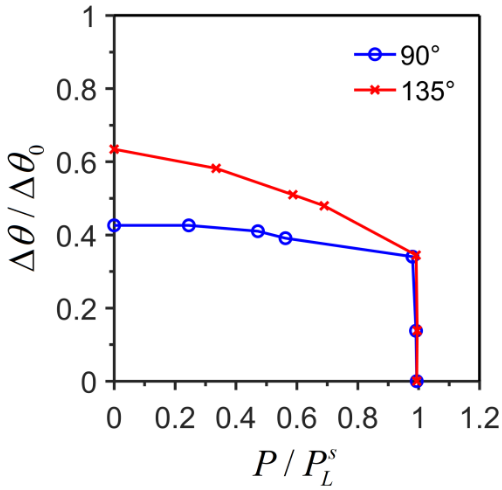


(d) Load condition 5

Fig. 17 Effect of bending radius on Shakedown limits under different load paths

*5.2 Effect of mean radius-thickness ratio ( $r/t$) on shakedown limits*

Taking 90° elbow pipe as an example, the influence of $r/t$ on shakedown limits is investigated in Fig. 18. This shows that some changes occur to the shakedown envelope over the thickness range considered. This is primarily because the magnitude of thermal stress created is relatively independent of thickness, with only thick pipes showing an increase in thermal stress.

The analysis of the results reveals a phenomenon different from the other cases, where the reverse plasticity limit values are almost the same regardless of the variation of the mean radius-thickness ratios (6, 10 and 15), as given in Fig. 18(a). As shown in Fig. 18, the shakedown limits of the pipeline with two elbow pipes with different mean radius-thickness ratios are significantly different under the five load conditions. And the shakedown limits of the three mean radius-thickness ratio the pipelines are clearly distinguished subjected to different coupled cyclic mechanical-thermal loading conditions.

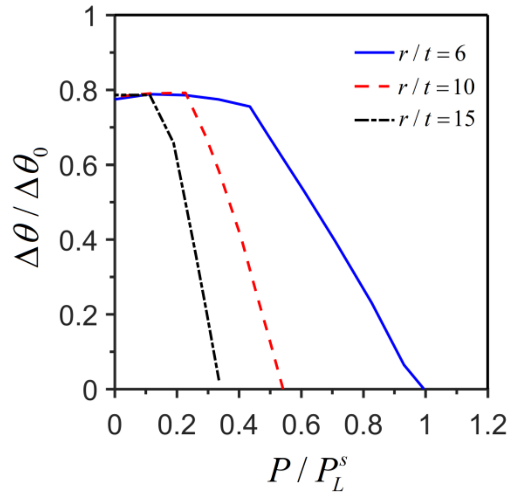


(a) Load condition 1

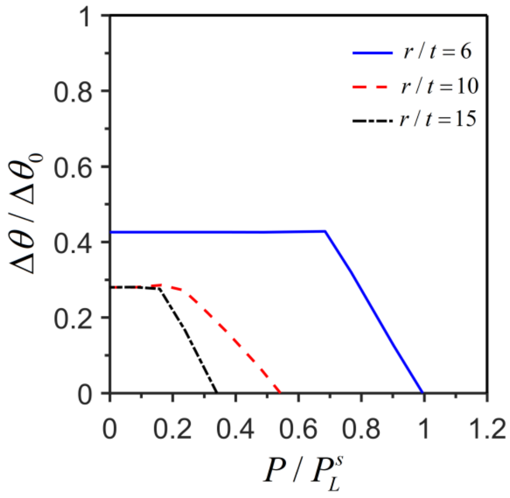


(b) Load condition 2

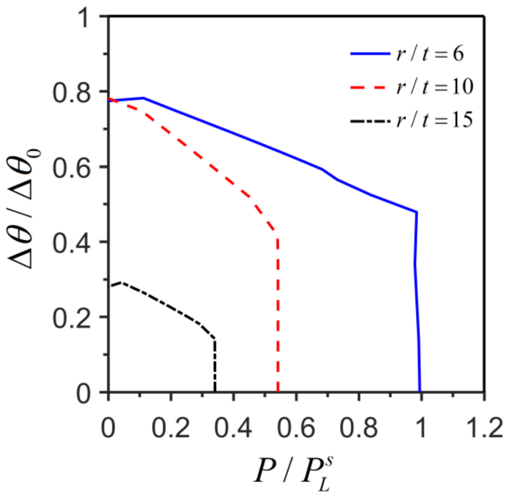


(c) Load condition 3

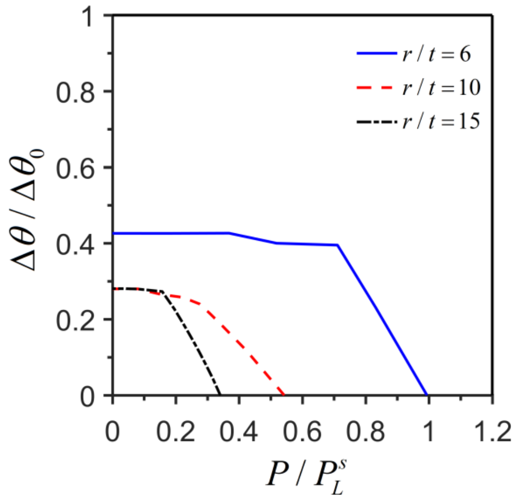


(d) Load condition 4

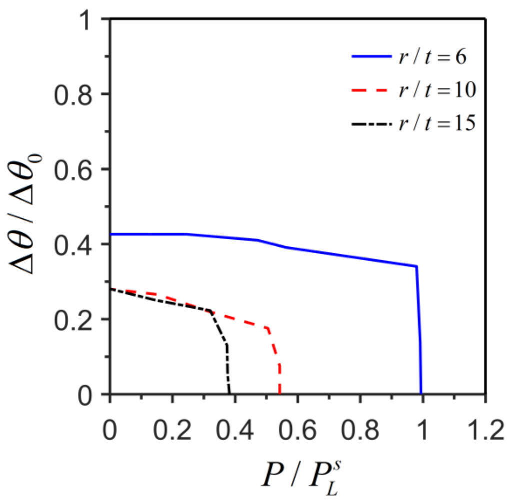


(e) Load condition 5

Fig. 18 Effect of radius-thickness ratio on shakedown limits of 90° elbow pipe

*5.3 Effect of load paths on shakedown limit*

Taking the 90° elbow pipe as an example, the influence of different coupled cyclic mechanical-thermal load conditions on shakedown limits is shown in Fig. 19. For load condition 2, load condition 4 and load condition 5, the shakedown limits are very similar to the part of the Bree diagram consisting of the reverse plasticity limit and the ratchet limit; and the analysis of the results reveals a phenomenon different from the other cases, where the reverse plasticity limit values of 135° elbow pipe ( $r/t=6$ ) is the same regardless of variations of loading conditions, as shown in Fig. 19(d). The shakedown limits of the 90° elbow pipes under load condition 1 and load condition 2 are clearly distinguished. It shows that the 90° elbow pipe has better structural stability under all these load conditions.

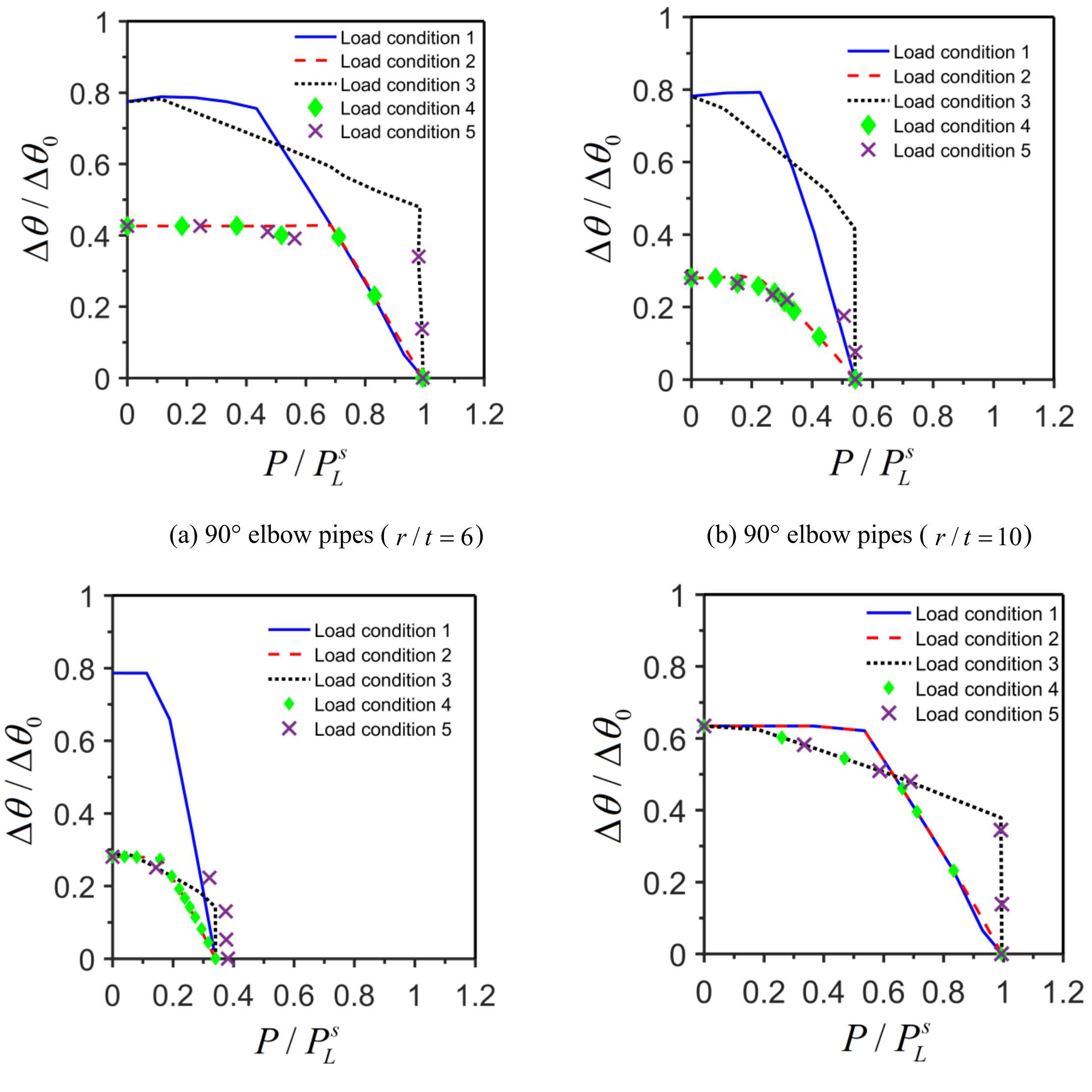


(a) 90° elbow pipes ( $r/t=6$ )　(b) 90° elbow pipes ( $r/t=10$ )

(c) 90° elbow pipes ( $r/t=15$ )　(d) 135° elbow pipes ( $r/t=6$ )

Fig. 19 Effect of load conditions on shakedown limits of 90° and 135° elbow pipe

**6. Conclusions**

In the research work, the thermal stress contour and displacement distribution of the elbow pipe under steady internal pressure and cyclic temperature load are firstly given. It is clear that the high stress is concentrated on the intrados of the elbow pipe. Secondly, the shakedown limits of 90° and 135° elbow pipes under coupled cyclic mechanical-thermal load conditions are determined by the linear matching method. Moreover, The ABAQUS incremental elastoplastic analysis is used to verify that the linear matching method can accurately give the shakedown limits of 90° and 135° elbow pipes under various load conditions and has great advantages in terms of high efficiency and convenience. Further, the influences of bending angles, mean radius-thickness ratio and five load conditions on shakedown limits are studied, respectively. The 90° elbow pipe has better structural stability under load condition 1. Therefore, the 90° elbow pipe should be selected as far as possible in practical engineering. The shakedown limits are very similar to the part of the Bree diagram consisting of the reverse plasticity limit and the ratchet limit. The effect of $r/t$ and load conditions on the shakedown limits of 90° and 135° elbow pipes is significantly different.

**Acknowledgments**

This work was partly supported by the Natural Science Foundation of Hebei Province of China (No. E2021501011), Central University Basic Scientific Research Business Expenses (No. N2123028), National Natural Science Foundation of China (52150710540).

**References**

[1] J. Li, C.Y. Zhou, P. Cui, X.H. He, Plastic limit loads for pipe bends under combined bending and torsion moment, Int. J. Mech. Sci. 92 (2015) 133–145. https://doi.org/10.1016/j.ijmecsci.2014.12.011.

[2] J. Li, C.Y. Zhou, J.L. Xue, X.H. He, Limit loads for pipe bends under combined pressure and out-of-plane bending moment based on finite element analysis, Int. J. Mech. Sci. 88 (2014) 100–109. https://doi.org/10.1016/j.ijmecsci.2014.07.012.

[3] S.J. Li, C.Y. Zhou, J. Li, X.M. Pan, X.H. He, Effect of bend angle on plastic limit loads of pipe bends under different load conditions, Int. J. Mech. Sci. 131–132 (2017) 572–585. https://doi.org/10.1016/j.ijmecsci.2017.08.019.

[4] S.Q. Xu, M.H. Yu, Shakedown analysis of thick-walled cylinders subjected to internal pressure with the unified strength criterion, Int. J. Press. Vessel. Pip. 82 (2005) 706–712. https://doi.org/10.1016/j.ijpvp.2005.03.003.

[5] C.S. Oh, Y.J. Kim, C.Y. Park, Shakedown limit loads for elbows under internal pressure and cyclic in-

plane bending, Int. J. Press. Vessel. Pip. 85 (2008) 394–405. https://doi.org/10.1016/j.ijpvp.2007.11.009.

[6] H.F. Abdalla, Shakedown boundary determination of a 90° back-to-back pipe bend subjected to steady internal pressures and cyclic in-plane bending moments, Int. J. Press. Vessel. Pip. 116 (2014) 1–9. https://doi.org/10.1016/j.ijpvp.2014.01.001.

[7] A.A. Oda, M.M. Megahed, H.F. Abdalla, Effect of local wall thinning on shakedown regimes of pressurized elbows subjected to cyclic in-plane and out-of-plane bending, Int. J. Press. Vessel. Pip. 134 (2015) 11–24. https://doi.org/10.1016/j.ijpvp.2015.08.003.

[8] H.F. Abdalla, M.M. Megahed, Validation of the Nonlinear Superposition Method (NSM) for elastic shakedown limit pressures via comparison with experimental test results of spherical vessels with radial and oblique nozzles, Int. J. Press. Vessel. Pip. 162 (2018) 19–29. https://doi.org/10.1016/j.ijpvp.2018.02.008.

[9] H. V. Do, H. Nguyen-Xuan, Computation of limit and shakedown loads for pressure vessel components using isogeometric analysis based on Lagrange extraction, Int. J. Press. Vessel. Pip. 169 (2019) 57–70. https://doi.org/10.1016/j.ijpvp.2018.11.012.

[10] H.F. Abdalla, A novel methodology for determining the elastic shakedown limit loads via computing the plastic work dissipation, Int. J. Press. Vessel. Pip. 191 (2021) 104327. https://doi.org/10.1016/j.ijpvp.2021.104327.

[11] R. Adibi-Asl, W. Reinhardt, Non-cyclic shakedown/ratcheting boundary determination - Part 1: Analytical approach, Int. J. Press. Vessel. Pip. 88 (2011) 311–320. https://doi.org/10.1016/j.ijpvp.2011.06.006.

[12] R. Adibi-Asl, W. Reinhardt, Non-cyclic shakedown/ratcheting boundary determination - Part 2: Numerical implementation, Int. J. Press. Vessel. Pip. 88 (2011) 321–329. https://doi.org/10.1016/j.ijpvp.2011.06.007.

[13] J.W. Simon, G. Chen, D. Weichert, Shakedown analysis of nozzles in the knuckle region of torispherical heads under multiple thermo-mechanical loadings, Int. J. Press. Vessel. Pip. 116 (2014) 47–55. https://doi.org/10.1016/j.ijpvp.2014.01.004.

[14] H.F. Chen, A.R.S. Ponter, Shakedown and limit analyses for 3-D structures using the linear matching method, Int. J. Press. Vessel. Pip. 78 (2001) 443–451. https://doi.org/10.1016/S0308-0161(01)00052-7.

[15] H.F. Chen, A.R.S. Ponter, Integrity assessment for a tubeplate using the linear matching method, Int. J. Press. Vessel. Pip. 81 (2004) 327–336. https://doi.org/10.1016/j.ijpvp.2004.02.016.

[16] H.F. Chen, A.R.S. Ponter, Integrity assessment of a 3D tubeplate using the linear matching method. Part 1. Shakedown, reverse plasticity and ratchetting, Int. J. Press. Vessel. Pip. 82 (2005) 85–94. https://doi.org/10.1016/j.ijpvp.2004.07.015.

[17] H.F. Chen, A.R.S. Ponter, R.A. Ainsworth, The linear matching method applied to the high temperature life integrity of structures. Part 1. Assessments involving constant residual stress fields, Int. J. Press. Vessel. Pip. 83 (2006) 123–135. https://doi.org/10.1016/j.ijpvp.2005.11.005.

[18] X. Zhu, H. Chen, F. Xuan, X. Chen, Cyclic plasticity behaviors of steam turbine rotor subjected to cyclic thermal and mechanical loads, Eur. J. Mech. A/Solids. 66 (2017) 243–255. https://doi.org/10.1016/j.euromechsol.2017.07.012.

[19] J.G. Gong, T.Y. Niu, H. Chen, F.Z. Xuan, Shakedown analysis of pressure pipeline with an oblique nozzle at elevated temperatures using the linear matching method, Int. J. Press. Vessel. Pip. 159 (2018) 55–66. https://doi.org/10.1016/j.ijpvp.2017.11.008.

[20] N.K. Cho, H. Chen, D. MacKenzie, D. Giugliano, Investigating the Effects of Cyclic Thermo-Mechanical Loading on Cyclic Plastic Behavior of a Ninety-Degree Back-to-Back Pipe Bend System, J. Press. Vessel Technol. Trans. ASME. 142 (2020). https://doi.org/10.1115/1.4043376.

[21] X. Zheng, H. Chen, Z. Ma, Shakedown boundaries of multilayered thermal barrier systems considering interface imperfections, Int. J. Mech. Sci. 144 (2018) 33–40. https://doi.org/10.1016/j.ijmecsci.2018.05.016.

[22] Z. Ma, H. Chen, Y. Liu, F.Z. Xuan, A direct approach to the evaluation of structural shakedown limit considering limited kinematic hardening and non-isothermal effect, Eur. J. Mech. A/Solids. 79 (2020) 103877. https://doi.org/10.1016/j.euromechsol.2019.103877.

[23] H. Peng, J. Shen, Y. Liu, H. Chen, Shakedown analysis of a torispherical head with a piping nozzle under combined loads by the stress compensation method, Int. J. Press. Vessel. Pip. 172 (2019) 107–118. https://doi.org/10.1016/j.ijpvp.2019.03.028.

[24] S. Balakrishnan, A.R. Veerappan, S. Shanmugam, Determination of plastic, shakedown and elastic limit loads of 90°pressurized pipe bends with shape imperfections, Int. J. Press. Vessel. Pip. 175 (2019) 103925. https://doi.org/10.1016/j.ijpvp.2019.103925.

[25] H. Chen, J. Ure, T. Li, W. Chen, D. Mackenzie, Shakedown and limit analysis of 90° pipe bends under internal pressure, cyclic in-plane bending and cyclic thermal loading, Int. J. Press. Vessel. Pip. 88 (2011) 213–222. https://doi.org/10.1016/j.ijpvp.2011.05.003.

[26] X. Chen, K. Huang, X. Zhu, H. Chen, M. Li, Ratcheting behavior of pressurized lateral nozzle of cylinder with local wall thinning under different loading paths, Eng. Fail. Anal. 117 (2020) 104947. https://doi.org/10.1016/j.engfailanal.2020.104947.

[27] H. Chen, Lower and upper bound shakedown analysis of structures with Temperature-dependent yield stress, J. Press. Vessel Technol. Trans. ASME. 132 (2010) 0112021–0112028. https://doi.org/10.1115/1.4000369.